NPDGamma Detector Array Technical Note

Michael Gericke

October 29, 2003

Contents

1   Introduction and Summary

The NPDGamma detector array has been designed to operate at noise levels that are low enough so that the time required to measure the asymmetry to the level of 5×10^{-9} is dominated by the collection of counting statistics. In addition, there should be no false asymmetries at the desired level of accuracy, due to the operation of the spin flipper in close proximity to the array or due to any spin flipper correlated electronic pickup. To ensure that beam off measurements of systematic effects can be made quickly compared to the time required to collect counting statistics, the detector efficiency, the number of photoelectrons produced in the vacuum-photodiode (VPD) per MeV, is desired to be reasonably high (> 500).

The average efficiency among all detectors was determined to be 1292 photo-electrons per MeV deposited in the crystal. The individual detector efficiencies fluctuated around this value by +/- 20%. This efficiency enters into the calculation of the average photo current seen at the detector preamplifier output. The time needed to measure a false asymmetry to a given accuracy is proportional to the inverse square of the average photo-current. LED's, which are located inside the detector scintillator crystal housing, were tested in each detector and light transmission properties for each crystal half were compared by alternating gamma exposure to each side and illumination from the LED on either side. The relative efficiency of the vacuum-photodiodes was tested in conjunction with the detectors to verify the VPD absolute efficiency measurement done at KEK [8]. This information was used to match the CsI crystals with the VPDs and select a suitable feedback resistor, used in the second preamplifier stage and, allow for gain matching between detectors at the desired level of uniformity (See section 3.4).

First long duration tests with the entire array, in conjunction with the DAQ system, were performed to establish the level of systematic effects in the calculation of the γ-asymmetry, measure the noise performance of the array and DAQ, as well as monitor any long term gain and pedestal fluctuations (See section 4). Any spin flipper correlated gain change in the VPD, possibly leading to a false asymmetry can only be seen with a signal going into the VPD. The LEDs were turned on to simulate the beam-on signal. The spin flipper was then turned on and data was taken with an average photo-current from the LEDs comparable to the expected beam-on current.

The time required to average the noise seen from the detector preamplifier during beam-off, LED off measurements was 3 hours.

False asymmetries were measured, with LED on and off, to the aforementioned accuracy within a few hours and were consistent with zero.

This note describes in detail the tests performed to address these issues and how the results compare to theory.

2 Detector Array Properties and Physics

Achieving the desired accuracy in measuring the parity violating gamma asymmetry relies on good counting statistics, with errors from other sources, such as electronic noise and other systematic effects comparatively small. In principle, the asymmetry could be measured using a single detector. However, using multiple detectors positioned to cover the largest cross-sectional contributions, coupled with good information about the angular position of the detectors not only detects more gammas but allows for a larger target as well, therefore shortening the time required to achieve the necessary counting statistics. To exploit as
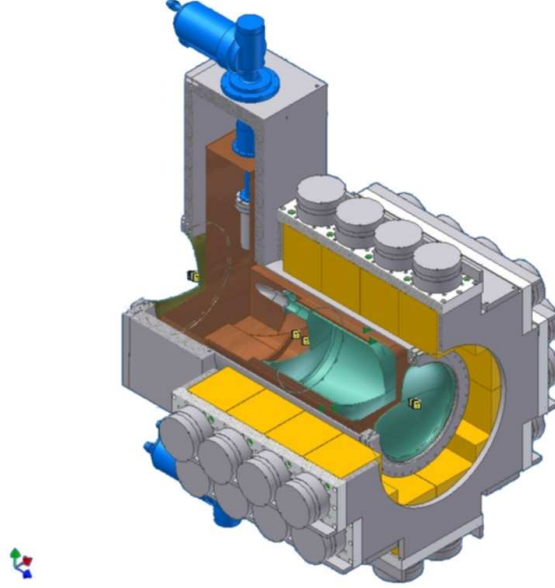

Figure 1: NPDGamma Detector Array and Target Assembly

much of the neutron beam and gamma cross-section as possible, the NPDGamma detector array consists of 48 detectors, arranged in a cylindrical pattern around the 20 liter liquid hydrogen target (Figure 1). Each detector consists of two rectangular pieces of optically coupled Thallium doped Cesium Iodide crystals. The overall dimensions are shown in figure 4. The crystal is encased in a 0.04 inches thick Aluminum housing and is coupled to a 3.00 *inch* diameter window at the top of the housing assembly to facilitate the detection of the produced scintillation light by a 3.00 inch vacuum photodiode (VPD) during standard operation. Each detector comes equipped with two light emitting diodes (LED); one in each detector half. The LED's are used during beam off detector diagnostic tests (See section 4.1.2).

   The particular type of vacuum-photodiode used was chosen for the low photo-cathode sheet resistivity. With an S-20 cathode, the VPD has a quantum efficiency of $\approx 10\%$ and 45mA/W radiant sensitivity at the CsI maximum emission wavelength (See table 1, section 7.1 and figure 2). Based on LANSCE FP12 beam brightness measurements and Monte Carlo calculations [1], the predicted gamma rate into a single detector is 20 MHz. At that rate, pulse counting is not possible. The detectors are therefore operated in current mode and the low sheet resistivity of the S-20 photo-cathode reduces the degree of gain non-linearities across its surface.
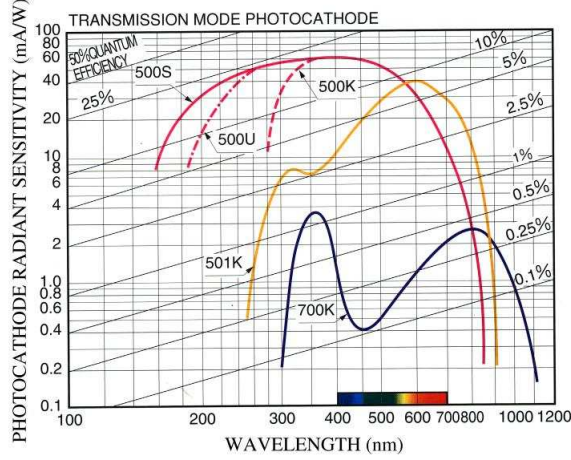
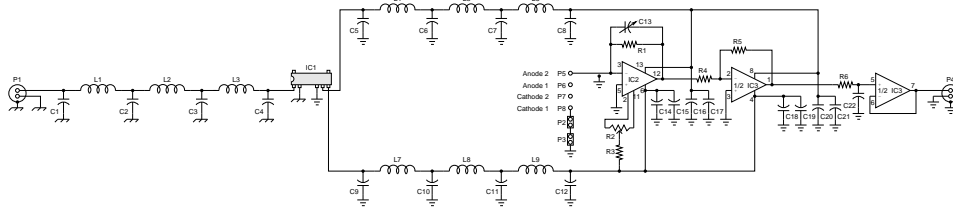Figure 2: Properties of S-20 (500K) photocathodes used

Figure 3: NPDGamma detector pre-amplifier

The cylindrical housing for the VPD and detector preamplifier has been designed to minimize noise contributions from capacitive coupling between electronic components and to shield the assembly from outside fields such as those produced by a radio frequency spin flipper used in the experiment [2]. A bias of 90 $Volts$ is applied across the VPD via two batteries located on top of the VPD and preamplifier housing. This ensures that the array can run for long periods of time while removing the necessity for an external supply to be connected directly to the VPDs.

The VPD current in each detector is processed by a low-noise preamplifier (See figure 3) [7]. The preamplifier output is connected to the NPDGamma DAQ, which incorporates 4 sum and difference amplifier boards with 12 channels each. Here, the detector signals are separated into an average of the 12 detector signals pertaining to a ring (See figure 1) and the difference between the actual detector signals in the ring and the average (See section 4.1.1). The 48 resulting difference signals and 4 sum signals are sampled by 5, 12 channel, 16 bit ADCs. The sampled data is transfered via fiber optic ethernet to a 3.5 Tbyte RAID array storage device.

The following is a short review of the underlying physical processes in sources of gamma-rays and their interaction with matter, as they relate to the tests described herein. A description of the setup, the procedures used in the various tests and the various results are given in the main sections (See table of contents).
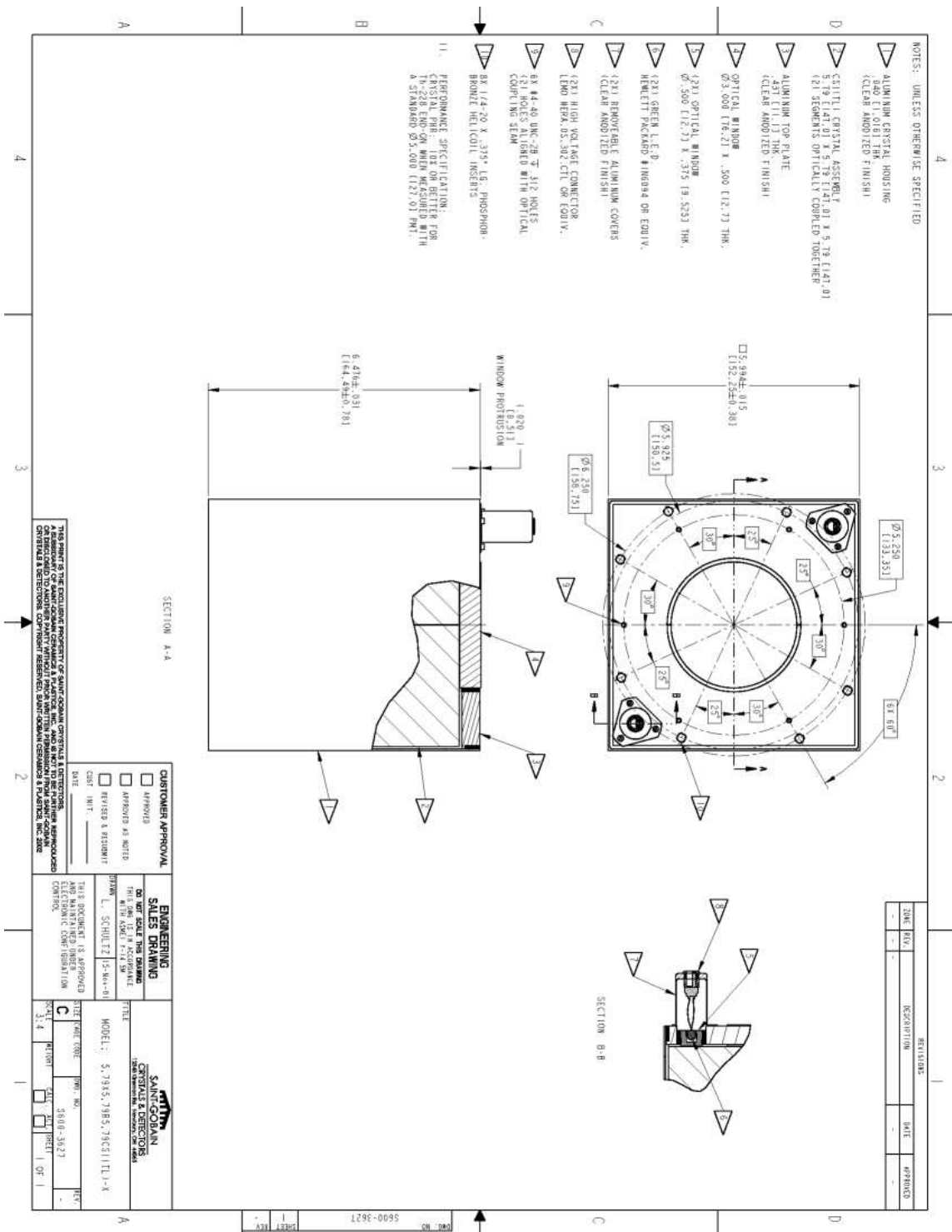
5

NOTES: UNLESS OTHERWISE SPECIFIED

1. ALUMINUM CRYSTAL HOUSING .040 [1.016] THK. (CLEAR ANODIZED FINISH)

2. CsI(Tl) CRYSTAL ASSEMBLY 5.79 [147.0] X 5.79 [147.0] X 5.79 [147.0] (2) SEGMENTS OPTICALLY COUPLED TOGETHER

3. ALUMINUM TOP PLATE .45T [11.1] THK. (CLEAR ANODIZED FINISH)

4. Ø3.000 [76.2] X .500 [12.7] THK. OPTICAL WINDOW

5. Ø.500 [12.7] X .375 [9.525] THK. OPTICAL WINDOW

6. (2X) GREEN L.E.D. HEWLETT PACKARD #1N6094 OR EQUIV.

7. (2X) REMOVABLE ALUMINUM COVERS (CLEAR ANODIZED FINISH)

8. (2X) HIGH VOLTAGE CONNECTOR LEMO #ERA.05.302.CTL OR EQUIV.

9. 6X #4-40 UNC-2B ⌴ .312 HOLES (2) HOLES ALIGNED WITH OPTICAL COUPLING SEAM

11. 8X 1/4-20 X .375 LG. PHOSPHOR-BRONZE HELICOIL INSERTS

PERFORMANCE SPECIFICATION: CRYSTAL PHR: 10% OR BETTER FOR Th-228 END-ON WHEN MEASURED WITH A STANDARD Ø5.000 [127.0] PMT.

SECTION A-A

SECTION B-B

WINDOW PROTRUSION

Figure 4: CsI Detector Physical Specifications.

2.1 Review

The emitted gamma-rays are the result of the transition of an excited nucleus to the ground state in at least one but possibly multiple steps, depending on the isotope at hand. In multiple step transitions, one gamma-ray for each step is emitted. In a radioactive element, the excited nucleus is usually left behind following the beta (^{137}Cs) or alpha (^{241}Am) decay of a parent nucleus. Since the energy difference between nuclear states is very well defined, the emitted gamma-rays are nearly mono-energetic.

In the interaction with matter, gamma-rays may transfer all or part of their energy to electrons within the material. How much of their energy they give to the electrons depends on the process of interaction. The three main processes involved in the interaction of gamma-rays with matter are photo-electric absorption, Compton scattering, and pair production. [3] In photo-electric absorption an incoming gamma-ray with the right energy will be absorbed by an atom in the material, in the process of which an electron is ejected. The energy of the electron is equal to that of the gamma-ray minus the binding energy of the electron in the atom $E_{e^-} = h\nu - E_b$. However, since the binding energy of the electron is on the order of eV while the energy of the photon will be on the order of at least keV the electron essentially has the energy of the gamma-ray. The probability of gamma-ray absorption depends on the atomic number of the nuclei in the material and is approximately given by

$$\tau \cong const \times \frac{Z^n}{E_\gamma^{3.5}}$$

Where n varies between 4 and 5. [3] This is the primary reason why high Z materials such as lead are used for gamma-ray shielding. The ejected electron will move through the material, exciting any atom in its path through collisions. Each atom will then de-excite by giving off a photon with an energy that depends on the specific atomic transitions in the material. For CsI(Tl) the emitted scintillation light has a wavelength centered around $550nm$ (See table 1, section 7.1). The number of atoms that are excited in this way depends directly on the kinetic energy of the electron and since the electron received all of its energy from the gamma-ray, the number of photons emitted from the material is a direct measure of the gamma-ray energy. The pulse counting method used (see below) to measure the number of photoelectrons per MeV relies on the accurate determination of the gamma peak position for the isotopes used.

The other common process is Compton scattering. In this case, the incident gamma-ray is not absorbed but scatters off a large number of electrons in the material. Each recoiling electron excites its host atom which then also de-excites by emitting a photon with a frequency that is characteristic of the material. However, in this case the energy given off to the electron may vary anywhere from zero to a large fraction of the gamma-ray energy. The energy of the scattered gamma-ray is given by

$$h\nu^s = \frac{h\nu}{1 + \frac{h\nu}{m_o c^2}(1 - cos(\theta))} \tag{1}$$

Where $m_o c^2$ is the rest-mass of the electron. Because of the many possible energies Compton scattered electrons may take on, the spectrum of any source due to this process will be washed out over a range up to the Compton edge, at which point Compton scattering decreases and photo absorption increases. The majority of scintillation light produced by the 2.23 MeV γ-ray, released in the $p(n,\gamma)d$ reaction, will be due to the Compton process.

In isotopes with closely spaced photo-peaks the Compton edge contributes to the spread seen in the photo-peak and distorts the resulting efficiency measurement. The sources used for the efficiency measurements described here are either low enough in energy to not have an appreciable Compton effect (^{241}Am) or have a photo-peak that is well separated from the Compton edge (^{137}Cs).

The excited electrons in the scintillation material will decay with a half-life of about a μs. Because the time it takes for the electron that was emitted in the process following the gamma-ray interaction to migrate through the material is much shorter
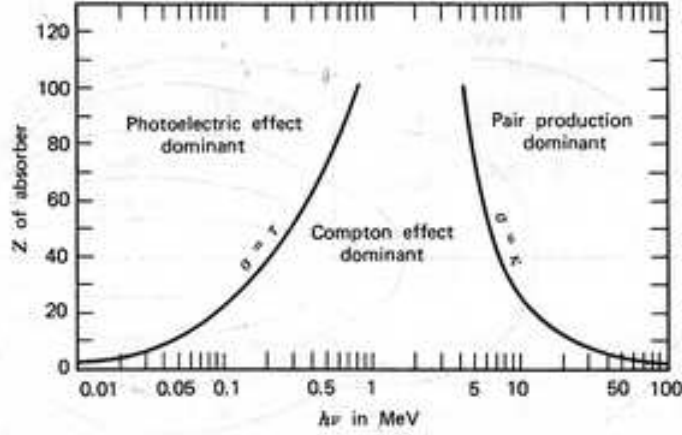

Figure 5: Relative contribution to scintillation from three major types of gamma-ray interaction.

than that, all the excited states are essentially formed at once and a large number of visible light photons will be emitted at nearly the same time with a spread determined by the above half-life. The light yield of CsI(Tl) is about 54000 Photons per MeV with a wavelength at maximum emission of $\lambda_{max} = 550$ nm and a scintillation efficiency of 11.9% [3] (See table 1 in the appendix).

At high gamma-ray energies, well above twice the rest-mass energy of an electron, the process of pair-production becomes probable. In this case, the photon is replaced by a positron-electron pair which will annihilate after slowing down, emitting two $0.511 MeV$ gamma-rays. Due to the low count rate from this process (as compared to photo-electric absorption) the peaks created from pair production can not be used to determine the CsI efficiency within a suitable time frame.

3 Detector Bench Tests

To establish the properties and performance of the individual detector components, a variety of tests were performed prior to their assembly.

The following sections give a detailed account of the tests performed in this mode.

3.1 CsI Relative Gain and Efficiency

The primary photo-peaks of two sources, $^{241}Am(10\mu Ci)$ and $^{137}Cs(6.75\mu Ci)$, were used to determine the number of photo-electrons per MeV (detector efficiency) from the peak

rms width. This procedure relies on the assumption that the photo-peak widths ($\sigma_p = FWHM/2.35$) observed from the MCA data are due primarily to the fluctuations in photo-electrons made at the photo-cathode and subsequent dynodes of the PMT (Shot noise), as well as crystal intrinsic properties. Additional contributions to the peak width due to electronic noise are lumped together with those due to crystal intrinsic properties into a single uncertainty σ_{int}.

The γ sources were placed approximately 6.8 *cm* away from the detector housing, centered on one side, so as to facilitate the equal γ exposure to both crystal halves (see figure 7).The γ-rays were collimated down to ~ 0.2 *sr*, using a 2 *inch* thick lead shield. The source was mounted on a special mount, designed to slide onto the detector, to ensure that the relative source-detector position is always the same. A 5 *inch* Hamamatsu R1513 PMT, used to take the source spectra was optically coupled to the detector window using various coupling compounds. Bicron's BCS 260 optical coupling grease was used for the detector efficiency measurements described here. A set of two randomly chosen detectors was later used in conjunction with two other coupling methods, to compare to the optical coupling grease.

The compounds were Dow Corning Sylgard 184 Silicone Elastomer Kit and Dow Corning high vacuum grease (clear). The ultimate decision which coupling material to use was based both on the increase of gain as compared to no coupling compound at all, as well as physical properties and ease of application (see section 3.3).

The PMT was supplied with 1.6 *kV* and its output was sent to a spectroscopic amplifier. The PMT signal was gain adjusted to produce a 4.0 *V* signal for the ^{137}Cs primary peak, as seen on the scope. The shaping time was 2 *μs*.
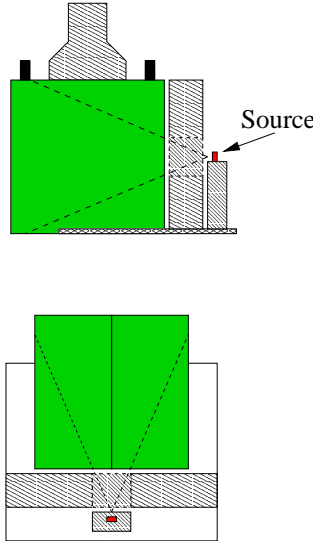
Figure 6: Detector Test Setup

The amplifier signal was sent to a multi-channel analyzer. The data collected by the MCA were transfered to a computer and further analyzed using computer programs. A block diagram of the detector electronics is shown in figure 7. A figure of the physical setup is shown in figure 6.

After acquiring the spectra of the two sources, the background subtracted photo-peaks were fitted with a Gaussian (see figure 8). The peak centroids are determined from the
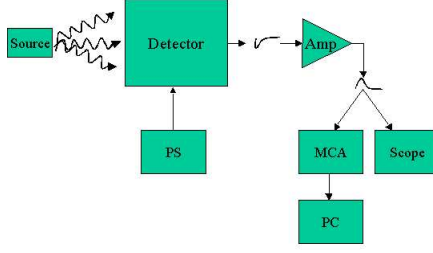
9

Figure 7: Measurement Setup Diagram

Gaussian fit as

$$m = ch_p \pm \frac{\sigma_p}{\sqrt{n}}$$

and the total number of counts for the peak is determined form the Gaussian integral as

$$n = \sqrt{\frac{\pi}{2}} \times cnt \times \sigma_p.$$

Where ch_p and cnt are the peak channel and the number of counts in that channel respectively. The peak centroids and knowledge of the energy of the emitted gamma-rays (0.06 MeV for ^{241}Am and 0.67 MeV for ^{137}Cs) were used to determine the energy zero-offset. To extract the efficiency, a plot of the peak variances versus inverse peak-energy was made (figure 8). A line was fitted to the data using a least-square fit.

$$\Sigma^2 = a\frac{1}{E} + \sigma_{int}^2 \tag{2}$$

Here $\Sigma = \sigma_p/m'$ where m' is the zero-offset corrected peak centroid. The slope of the line

$$a = \frac{1}{N}(1 + \frac{1}{\delta - 1})$$

(See section 6) determines the number of photoelectrons per MeV as

$$N = a^{-1}\frac{\delta}{\delta - 1} \simeq \frac{1.37}{a}.$$

Where δ is the Poisson distributed gain in the number of electrons produced at the PMT cathode which, for a 10 stage Hamamatsu R1513 PMT operated at $1.6kV$, is ~ 3.7. The overall gain for the PMT used is 5×10^5 at $1.6kV$. Errors have been determined according to the standard procedures used in least-square fits (see for example [5]). The error on the peak variances (Σ^2) is calculated from

$$\delta\Sigma^2 = \pm \left(\frac{\sigma_p}{m'}\right)^2 \frac{\sqrt{2\frac{\sigma_p^2 m'^2}{n} + 2}}{m'}.$$

The event counting time for each source and detector was $300s$. The activities for (^{137}Cs) and (^{241}Am) were approximately $6\mu Ci$ and $10\mu Ci$ respectively.

The counting statistics for the time counted are therefore $\sim 0.1\%$ for (^{241}Am) and $\sim 0.07\%$ for (^{137}Cs). The overall error on the efficiency values was dominated by the quality of the least-squares fit.
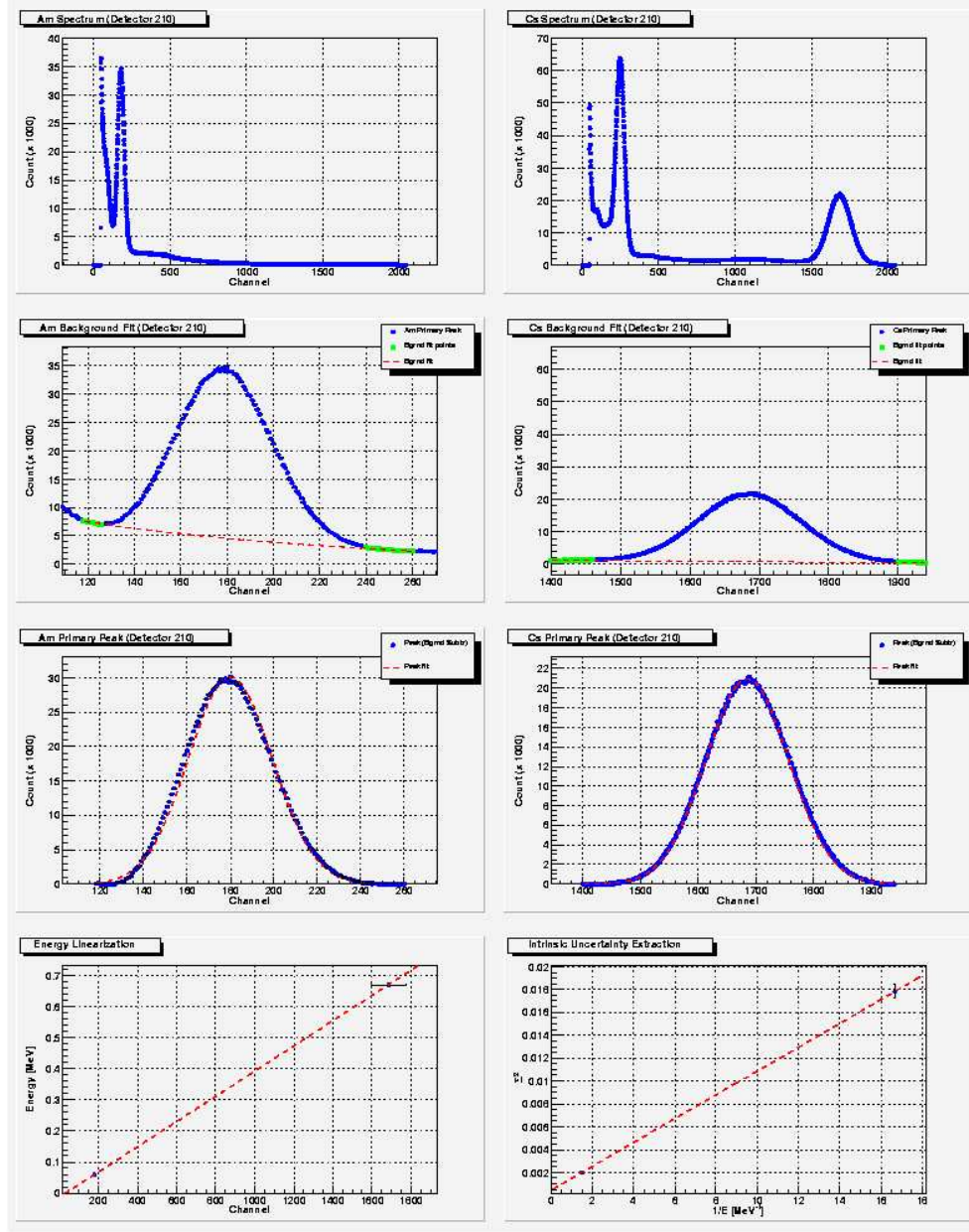
10

Figure 8: Detector Efficiency Extraction

To ensure that the CsI scintillators have uniform gain properties when comparing their two crystal halves (See figure 4), each half was exposed to the ^{137}Cs source and the spectroscopic amplifier voltage was monitored on the scope. Measurements were taken with the source on the left side, right side and the center of the scintillator, where the center is defined as in the configuration in figure 6. According to this method, it was found that, in the worst case, the gain varies by about 7% from one crystal half to the other. The results are shown in figure 9. The gains shown there have been normalized to the values measured when the source is centered on the seam between the two crystal halves (center position).
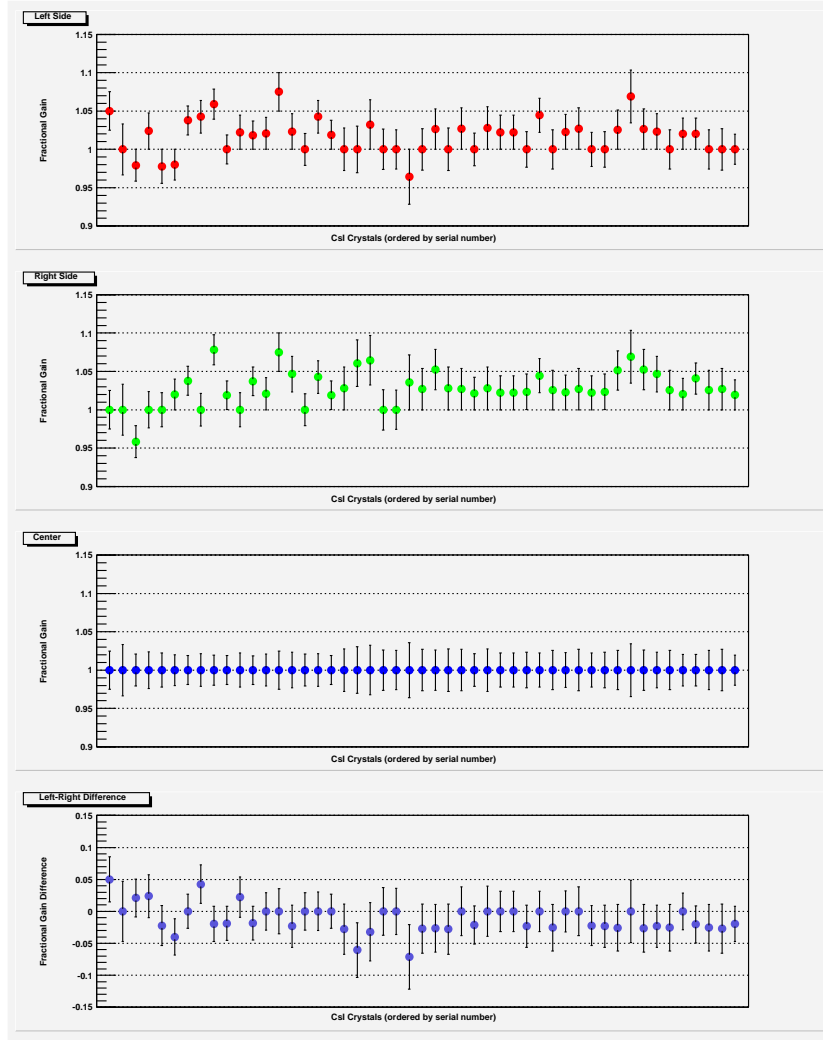
Figure 9: Differences in left and right side Crystal gains for each detector.

The efficiency measurements produced an average of 1292 photoelectrons per MeV with an overall variation of 40% between detectors. Figure 10 shows the results for 48 detectors in the order they were taken. The error in the values is about 5%, mostly due to the least squares fits used. The relative detector gain, as recorded from the scope is shown in figure 11

The efficiency results are used in conjunction with VPD relative efficiency, measured in a neutron beam at KEK [8], to match the overall gain between individual CsI-VPD detector assemblies. Relative VPD gain was again measured at Los Alamos, using the LED's in the CsI(See section 3.2). The purpose is to match the CsI with the VPDs in such a way that a reasonable range of feedback resistors in the detector preamplifier can be used to match the detector gains at the few percent level (See section 3.3). To produce such a close match, the error bars on the individual detector gain measurements have to be reduced. Measuring the overall gain of the VPD-CsI assembly will remove the need to use the fitting procedures described in the previous section and should therefore produce more accurate results (See section 3.4).
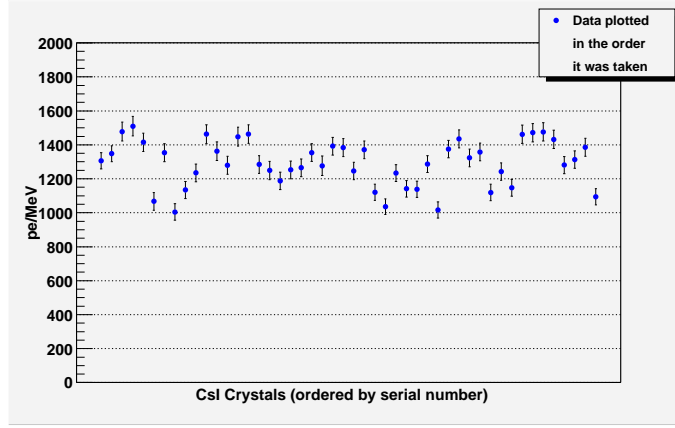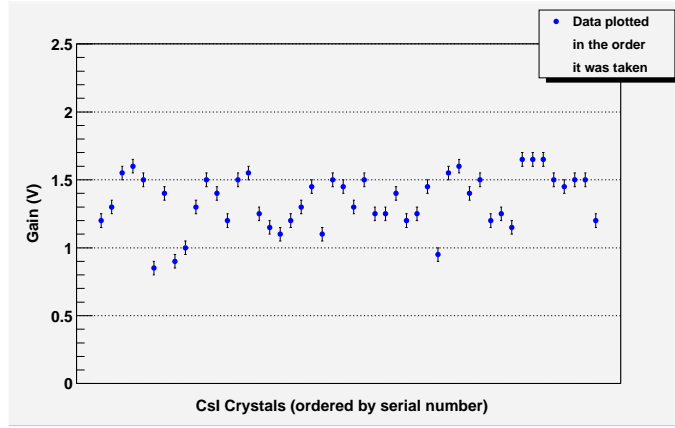
Figure 10: CsI Detector Efficiency

Figure 11: Detectors Relative Gain Shifts From Scope

3.2   LED and VPD Tests

The LED tests performed served three main purposes:

1. make sure the LEDs work

2. provide a line of comparison for later use of LEDs in diagnostic tests (See section 4.1.2)

3. be able to match the CsI crystals and the VPDs to obtain a reasonably uniform relative gain between detectors

The LEDs in each crystal were tested in conjunction with the VPDs, using a 100 Hz square-wave pulse signal. The LED driving voltages necessary to produce three different preamplifier output voltages $(-1\ V,\ -15\ V,\ -10\ V)$ were recorded. Each crystal half was tested individually with the LED on its side, as well as both sides together. This served to verify the functionality of the LEDs as well as the complete detector assembly, however no relative measurement can be made in this way. These tests were performed using no optical coupling component between the crystals and the VPDs. To test for the relative VPD efficiency, a single CsI crystal was combined, in turn, with each VPD, using vacuum grease as coupling (See section 3.3). A $2V$, 100 Hz square wave was applied to both LEDs

13

in the crystal and kept constant. The current drawn by the LEDs was monitored and was seen to remain constant at about 18.5 mA throughout the testing for all 50 VPDs tested. A picture of the VPD test setup is shown in figure 12 Absolute gain measurements for the
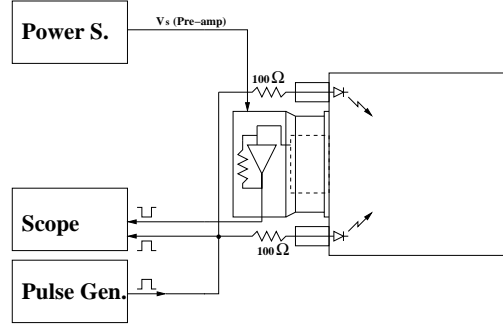

Figure 12: VPD and LED Test Setup

VPDs can not be made using the this procedure, since we have no information about the amount of light that is produced by the LEDs. The results are shown in figure 13. These
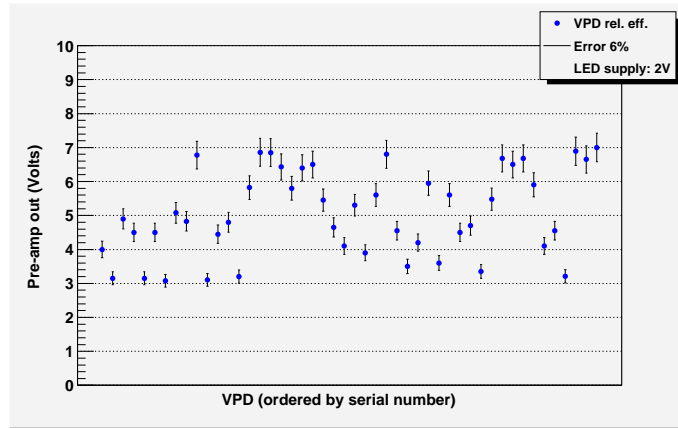

Figure 13: VPD relative efficiency results from Los Alamos tests.

measurements are compared with those done at KEK [8] in Japan, where a calibration measurement of the VPD's was done in conjunction with one CsI crystal, facilitating the neutron radiative capture in Cd and In targets. The scatter plot in figure 14 shows that the two measurements mostly agree to within errors. The scatter is most likely due to the change in optical coupling quality when switching the VPDs.

3.3 CsI-VPD Matching

As already mentioned, the CsI and VPD efficiencies are used to pair them in such a way as to reduce the overall gain variations between them. A few other components in the overall assembly play a role in determining these variations as well. After the individual gain differences seen between VPDs and CsI crystals, perhaps the most significant gain shifts can be introduced via the quality of optical coupling between any VPD-CsI pair. Different coupling
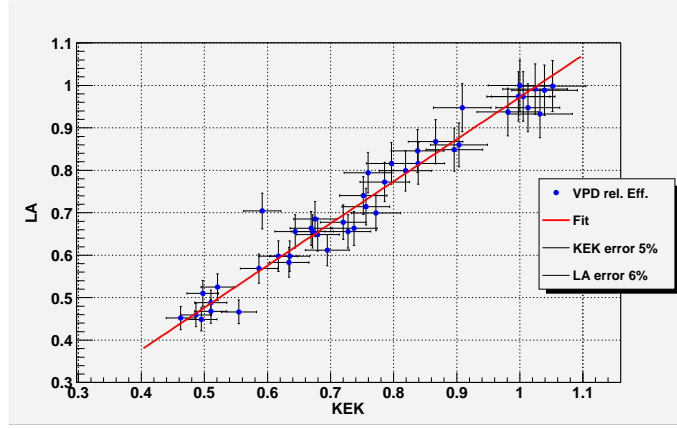
14

Figure 14: KEK vs. Los Alamos VPD relative efficiency results

methods and components produce varying results. The various compounds mentioned in section 3.1 were tested as to their influence on the overall detector gain, as compared to no coupling at all. During testing, in each setup a pair of detectors was randomly chosen and tested with all three optical coupling methods. Namely,

1. BC 630 Bicron optical coupling grease,

2. Dow Corning Sylgard 184 Silicone Elastomer (Cookies) and

3. high vacuum grease (translucent).

The Sylgard elastomer was used to make "cookies", circular $3inch$ diameter disks, about $3mm$ thick. The initially fluid compound was produced in a small dish and was positioned in a closed container which was subsequently evacuated until the vast majority of air boiled off. The compound was then poured into a cast with small air holes and then allowed to set, standing on its side. In this fashion, a maximum flatness off the surfaces in contact with either the CsI window or the VPD could be achieved. Unfortunately, even minute non-uniformities in the surfaces of the VPD window, as well as scratches on the surfaces of the cast that left their imprint on the "cookie" kept them from producing significantly better results than using no coupling at all. The best use for the Sylgard elastomer is in cases where it can be poured into place with the scintillator and VPD or PMT and is allowed to settle in that configuration without being disturbed. However, this option was not considered because the detector array configuration in the experiment makes it difficult to exchange entire CsI-VPD assemblies in-situ.

The best results were obtained using Bicron's optical coupling grease. With respect to it, the gain was reduced by a factor of two when no coupling component was used at all. The "cookie" method produced about 60% of the gain achieved with BC 630. The concern with BC 630 is that it has a relatively low viscosity and might run, leaving air pockets between the VPD and the CsI window. This is especially problematic for those detectors that sit in the array while being rotated on their side.Translucent high vacuum grease was used in the same fashion as the BC 630 grease. The gain measured was 90% of the gain measured with BC 630. However, the viscosity of the vacuum grease is much greater than that of BC 630. The high vacuum grease was therefore chosen as a good compromise.

Figure 15 shows the gain ordered efficiency test results for the VPDs (Green), the CsI crystals (Red) and their product (Blue). The blue curve is thus a theoretical prediction.

15

The actual relative gain shifts are expected to differ form this prediction, due to variations in optical coupling quality among the detectors. Nevertheless, the CsI crystals were matched with the VPDs according to the configuration presented in the figure. This served as a starting point from which to conduct additional efficiency measurements and further improve the gain via the adjustment of the feedback resistors in the detector preamplifier. At this stage, all feedback resistors in the preamplifier (See figure 3) were identical for
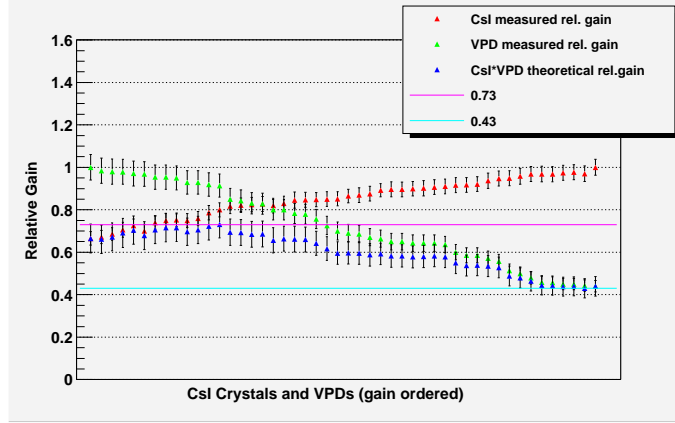

Figure 15: CsI and VPD gain matching

all detectors. The overall variation seen in the efficiency measurements performed on the completely assembled detectors (Section 3.4) determine the change in feedback resistance necessary to adjust the gain in any given detector.

3.4 Combined Relative Gain Tests

To compare the predicted values for the relative gain between detectors, the assembled detectors underwent a bench-test in which the ^{137}Cs source was used produce a current mode output. The corresponding preamplifier output was fed through a low-pass filter and monitored with a precision voltmeter. The source was located flush with the outside surface of the detectors and centered on one side. A source with the given activity (See section 3.1) and in the given configuration (Solid angle $\simeq 0.4$) is expected to deposit approximately 6.54×10^4 MeV/s into the detector. With the measured average CsI efficiency of ~ 1300 pe/MeV one expects to measure an output on the order of a few millivolt. To measure these outputs at the few percent level requires the preamplifier output to be very stable. However, even the op-amps used in the detectors will fluctuate at this level. The low-pass filter used was adjusted to have a time constant of *15 seconds* to try and stabilize the voltage. Later measurements, performed on the entire array, used a Lock-In amplifier and a stronger source to reduce the error on the gain values measured (See later this section). Three measurements were taken for each detector, one without source, one with source in place, and again without the source, in that order. These were taken sufficiently quickly so as to block fluctuations with long time constants (minutes). Figure 16 shows the difference between the signal with source and the average of the two signals taken without the source, versus detector serial number.

The overall spread in gains is still $\sim 40\%$, but the relative gains have shifted a bit, as expected.
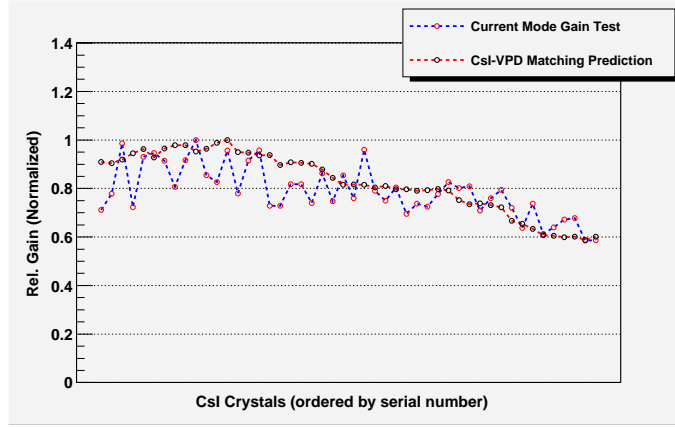
Figure 16: Detector current mode relative gain test results.

A collection of resistors in the range 1.50 $k\Omega$ to 2.80 $k\Omega$ is then used to replace the 2.15 $k\Omega$ resistors which had been installed in the second amplifier stage. The desired result is to match the detectors at the few percent level to ensure that the ADC channels for the detector difference signal do not saturate. To achieve this accuracy, several iterations of tests will be performed, after which the resistor values are adjusted accordingly. Given the range and accuracy of the resistors used and without taking into consideration other causes leading to changes in relative gain, the gain matching achievable, in principle, is shown in figure 17 (red curve). The realistic level of matching is governed not only by the feedback resistor values but also by changes in optical coupling quality (see section 3.3), as well as any time dependent gain fluctuations in the detectors.
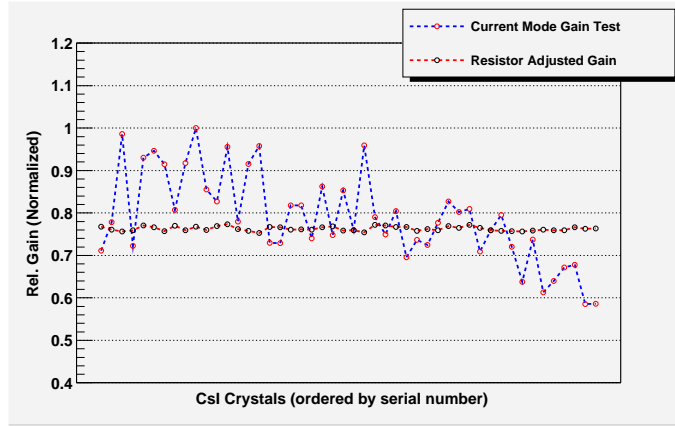

Figure 17: Resistor adjusted relative detector gains.

4 Detector Array Tests

In conjunction with the data acquisition, the entire array can now undergo tests that will help establish the degree of long term fluctuations in detector pedestals, gain stability and electronic noise due to changes in the environment, such as temperature fluctuations and changing magnetic fields from the spin flipper and other sources. In the final configuration, the spin flipper is mounted very close to the detectors and during normal operation, when the signal out of the VPDs is large, the multiplicative effect on the gain, of any magnetic fields leaking into the VPDs, can have significant systematic effects. This is especially true since the change in gain would be correlated with the spin reversal of the neutrons and may lead to false asymmetries. Using the LEDs in each of the detectors and the DAQ, we can simulate large signals going into the VPDs and test the effect of running the spin flipper on asymmetry measurements. In addition, more accurate measurements of the absolute detector gain can now be made through the use of stronger sources, lock-in-amplifier techniques and by observing the gain over longer periods of time. Background due to cosmic rays incident on the array crystals is also measured in this mode.

This section describes these tests and establishes a set of diagnostics that will be used to establish the state of the array at any given time during the experiment. The first order of business is to verify that the noise levels in the array and DAQ are consistent with the electronic noise at the Johnson level. The accuracy of every measurement mentioned above has to be viewed in relation to the noise levels in the detector pedestals. To this end, it is necessary to obtain large sets of data to establish good statistical accuracy with a minimum of time required to measure the contributions from systematic errors.

4.1 Detector Electronic Noise and Beam Off False Asymmetry

In a current mode experiment, the accuracy of the measurement is governed by the rate and quality of sampling of a signal that may be viewed as a continuous string of specific values of a random variable. The randomness and the spread (*rms* width) of the samples determines how many samples one must take to achieve a certain level of accuracy in a measurement, while the sampling rate determines how long that will take and whether or not one has in fact measured a representative subset of the process.

The correlation between samples taken at different times contributes to the overall width of the distribution obtained after extended sampling. This correlation is, of course, ultimately determined by the method of sampling, and over sampling will produce larger variances in the results. Under sampling, on the other hand, will cause an undesirable increase in the time required to achieve counting statistics.

During normal operation, the noise in the detector array, must be dominated by the shot noise due to the fluctuations in the number of photo-electrons created at the VPD photo cathode for a given *γ-ray* going into the detector. In other words, the time required to measure the asymmetry to the proposed level of accuracy must be governed by the time it takes to achieve the necessary counting statistics. During beam-off measurements, the time required to determine any systematic effect such as asymmetries due to electronic noise is governed by the noise in the preamplifier and the rest of the DAQ (Johnson noise). Since the experiment seeks to determine the asymmetry at the 5×10^{-9} level, any systematic effect resulting in a false asymmetry has to be measured to at least this level of accuracy

and in a short period of time.

The detector preamplifier (See chapter introduction) and the rest of the DAQ was designed under the requirement that there be no additional noise contribution beyond the expected Johnson noise from the first preamplifier stage [7]. The subject of this section is the theoretical prediction of the electronic noise we expect to see at the end of the analysis chain, based on the above assumptions, as well as the measurements performed to verify this prediction.

4.1.1 Detector Noise

The thermally excited motion of the free electrons in a conductor produces random voltage pulses on a very short time scale. At any given instant, a large number of these pulses contribute to produce a particular voltage drop across this conductor. The values measured are random and, from the central limit theorem, are expected to fluctuate according to a Gaussian distribution, around some DC voltage offset. Because of the short duration of the individual pulses making up the measured voltage drop, the spectral density (power spectrum) is approximately flat [4] ($\mathcal{S}_{V_J}(f) \simeq \mathcal{S}_{V_J}(0)$).

For the purposes of noise analysis, the most important component of the detector preamplifier circuit (See figure 3) is the first amplifier stage connected to the VPD anode. The stage incorporates a $50M\Omega$ feedback resistor which is expected to produce the largest component of noise, by far. While also producing noise, subsequent resistors in the DAQ stream are so much smaller in resistance (by 3 orders of magnitude) that their noise contribution is expected to be negligible. However, each additional amplifier and filter stage in the DAQ will have a multiplicative effect on the the noise generated in the first stage.

Such amplifier stages are referred to as fixed parameter linear systems; i.e. the output of the system depends on the parameter(s) in the same way as the input to the system and such a system could be described by a set of linear differential equations. Most basic electronic circuits fall under this category (See for example [4]). Each such system has associated with it a system function $\mathcal{H}(i\omega)$ which relates the input ($\mathcal{X}(i\omega)$) to the output ($\mathcal{Y}(i\omega)$) of the system

$$\mathcal{Y}(i\omega) = \mathcal{H}(i\omega)\mathcal{X}(i\omega).$$

Here the input and output is expressed as the Fourier transform of the relevant time dependent signals.

For the relation between the input and output power spectra, we also have

$$\mathcal{S}_y(\omega) = |\mathcal{H}(i\omega)|^2 \, \mathcal{S}_x(\omega).$$

In the case of a noisy resistor we have a system function which relates output current noise to the input voltage noise; i.e current fluctuations seen due to random variations in voltage drop across the resistor. One can use several different equivalent circuits to describe a noisy resistor. One such system is a noiseless resistor connected in series with a regular inductor, across a voltage source (V_J) [4]. Since the variance of a signal due to a stationary random process is equal to the intensity of its time varying component, the power dissipated in the model circuit can be expressed as

$$\langle x^2 \rangle = \int_{-\infty}^{\infty} \mathcal{S}_x(f) df.$$

Or, for the equivalent RL circuit

$$\frac{L}{2}\langle I^2 \rangle = \frac{k_B T}{2} = \int_{-\infty}^{\infty} \mathcal{S}_{I_J}(f)df.$$

The appropriate system function for this circuit is

$$\mathcal{H}(i\omega) = \frac{1}{\sqrt{R^2 + (i\omega L)^2}}.$$

So one finds that

$$\mathcal{S}_{I_J}(f) = \frac{\mathcal{S}_{V_J}(f)}{R^2 + 4\pi^2 f^2 L^2}$$

and

$$\langle I^2 \rangle = \frac{k_B T}{L} = \int_{-\infty}^{\infty} \frac{\mathcal{S}_{V_J}(f)df}{R^2 + 4\pi^2 f^2 L^2} = \frac{\mathcal{S}_{V_J}(0)}{2RL}. \tag{3}$$

Therefore, the noise due to thermal excitation out of the first amplifier stage is predicted to be

$$\mathcal{S}_{V_J}(0) = 2k_B T R. \tag{4}$$

Note that, were one to integrate from 0 to ∞ in equation 3 one would recover the usual result for Johnson noise with an additional factor of two.

This noise is expected to change further, due to additional filtering stages and due to the particular sampling rate used in the DAQ. In fact, while the answer sought is the rms width seen in the per-amplifier output, one has to determine the effects of filtering in the DAQ to establish a suitable sampling rate, to find the correct bandwidth for the theoretical prediction of the noise levels and to be able to relate the noise seen in the data stream back to the noise at the first preamplifier stage.

For single low pass filter, the expected *rms* width in the noise would be

$$\langle V_{rms} \rangle = \sqrt{\int_{-\infty}^{\infty} \frac{2k_B T R \, df}{1 + \omega^2 R^2 C^2}} = \sqrt{2\pi k_B T R f}.$$

To gain information about the sampling rate that should be used for such a system, based on the filter bandwidth used, one can calculate the auto-correlation function; i.e. the correlation between samples taken at different times. Thus, we have

$$\begin{aligned}
\mathcal{R}_{I_J}(\tau) &= \langle V_J(t) V_J^*(t + \tau) \rangle \\
&= \int_{-\infty}^{\infty} \frac{e^{2\pi i f \tau} \mathcal{S}_{V_J}(f) \, df}{1 + 4\pi^2 R^2 C^2 f^2} \\
&= \frac{k_B T}{C} e^{-|\frac{\tau}{RC}|}
\end{aligned}$$

$$\tag{5}$$

where $\mathcal{R}_{I_J}(\tau)$ is the Fourier transform of the power spectrum $\mathcal{S}_{I_J}(\omega)$.

According to this result, for an RC filter with $\omega = 5 \; kHz$ the correlation between time samples falls to 10% of its maximum value at a sampling period of $\simeq 0.43 \; ms$ and is nearly zero at a period of $\simeq 1 \; ms$.

In the NPDGamma DAQ system, the signal from the detector preamplifier is processed by feeding it through a 6 pole Bessel filter [6] in which each pole can be approximated by

a simple RC low pass filter system function, as it was used above. The auto-correlation function is then

$$\mathcal{R}(\tau) = 2k_B T R \int_{-\infty}^{\infty} \frac{e^{2\pi \ if\tau} \ df}{(1 + 4\pi^2 R^2 C^2 f^2)^6} \tag{6}$$

Before this happens, however, an average for each ring in the array is computed and each detector signal has its corresponding ring average subtracted. The process is shown schematically in figure 18. Here each difference amplifier contributes a gain factor of *10* and each Bessel filter stage (denoted by F in the schematic) contributes an additional factor of *3* to the gain. The sum and difference signals are sampled at 50 kHz for a duration of 40 ms, followed by a 10 ms brake, before the next macro pulse is sampled. This results in 2000 samples taken for each macro pulse. In the data stream (before the raw data is written to file) every group of 20 samples is summed to produce a final value for each of 100, 0.4 ms wide time bins. According to figure 18 and the sampling scheme just described, the data
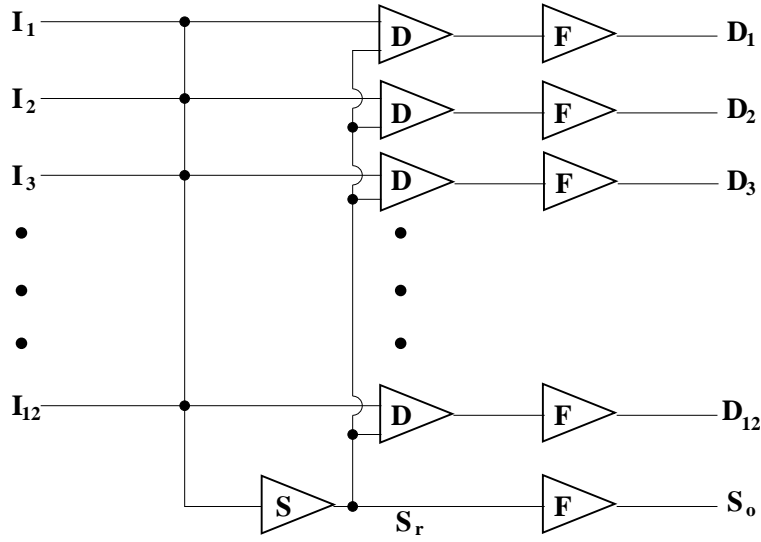

Figure 18: DAQ sum and difference amplifier schematic.

actually stored are the 48 difference signals from each detector $D_{d,i} = 20 \ D_i$ and the 4 sum signals corresponding to each detector ring $S_d = 20 \ S_o$. here $D_i = 30(I_i - S_r)$ and $S_o = 3 \ S_r$ are the signals sampled by the DAQ ADCs.

The auto-correlation function for the 6 pole Bessel filter is shown in figure 19. The blue, curve shows the correlation between samples taken at different times when no particular sampling scheme is considered. The red curve takes sampling into consideration (see below). The graph shows that, at the chosen sampling rate, the correlation between samples is almost at its maximum and any data taken at that rate, when taken as is, will show variances that indicate a higher noise level than actually present. However, the picture changes when one integrates the signal as described above. With the sampling scheme described above, the setup follows what is referred to as the periodic sampling of a random variable, in which each macro pulse describes an individual sample function. Each of those sample functions exhibits essentially the same statistical behavior (follows the same distribution function), which makes the process ergodic. A typical example of a detector pedestal output is shown
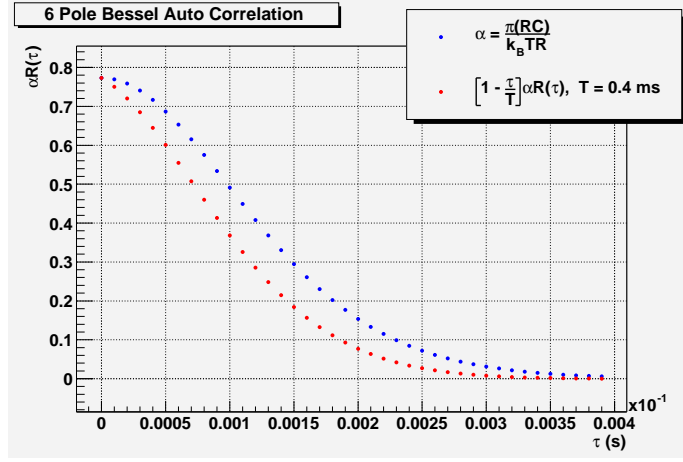
21

Figure 19: Auto-Correlation function for a 6 pole bessel filter.

in figure 20. Under these circumstances, the variance in the detector signal is [4]

$$\sigma^2(V) = \frac{2}{T} \int_0^T \left(1 - \frac{\tau}{T}\right) \mathcal{R}(\tau) \, d\tau \tag{7}$$

Where $\mathcal{R}(\tau)$ is given by equation 6.

Here τ is the time difference between the initial sample and any subsequent sample taken during the sampling interval T. So in the calculation of the relevant statistic (mean, standard deviation, etc ...), if we take an individual time bin measurement as the fundamental random variable then $T = 0.4 \, ms$ and $\mathcal{R}(\tau)$ will be the correlation between all ADC samples within that time bin. On the other hand, if we integrate over an entire macro pulse and take that value to be the fundamental quantity then $T = 40 \, ms$ and $\mathcal{R}(\tau)$ will be the correlation between all ADC samples within that macro pulse. Figure 19 shows that any measurement taken in one time bin is statistically independent from any measurement taken in any other time bin. In lite of this one can conclude that either of the two analysis methods described will work. How is the correlation between samples and, therefore, the *rms* width seen in
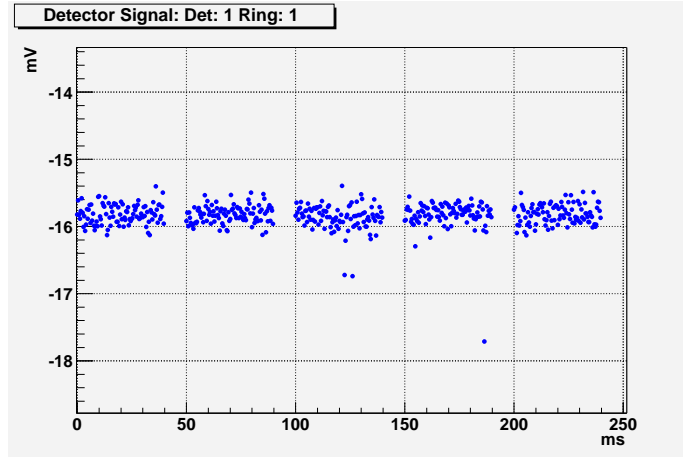

Figure 20: Typical detector pedestal signal.

the data, changed by the sum and difference amplifier? If we start with the expected power

22

spectrum seen in an individual detector, we can propagate the signal through the circuit to establish what we see in the data and then relate it back to what we started with.

For the sum signal in a given ring we have

$$V_{S_r}(t) = \frac{1}{12}\sum_{i=1}^{12} V_{I_i}(t)$$

and, since the samples taken from different detectors are statistically independent (the detectors and the DAQ channels are electrically isolated), the auto-correlation for the sum signal is

$$\langle V_{S_r}(t)V_{S_r}^*(t+\tau)\rangle = \frac{1}{(12)^2}\sum_i \langle V_{I_i}(t)V_{I_i}(t+\tau)\rangle$$

$$\mathcal{R}_{S_r}(\tau) = \frac{1}{(12)^2}\sum_i \mathcal{R}_{I_i}(\tau)$$

$$\Rightarrow \mathcal{S}_{S_r}(\omega) \simeq \frac{1}{12}\mathcal{S}_{I_i}(\omega)$$

$$(8)$$

So the noise seen in the sum signal is approximately equal to $1/12$ the noise seen in any individual detector of that ring, provided that the noise in each detector is about the same.

For the difference signal, we have

$$\langle V_{D_i}(t)V_{D_j}^*(t+\tau)\rangle = (30)^2(\langle V_{I_i}(t)V_{I_j}^*(t+\tau)\rangle$$
$$+ \langle V_{S_r}(t)V_{S_r}^*(t+\tau)\rangle$$
$$- \langle V_{S_r}(t)V_{D_j}^*(t+\tau)\rangle$$
$$- \langle V_{D_i}(t)V_{S_r}^*(t+\tau)\rangle)$$

Which, using equation 8, gives

$$\mathcal{R}_{D_i}(\tau) = (30)^2\left(\mathcal{R}_{I_i}(\tau) + \mathcal{R}_S(\tau) - \frac{2}{12}\mathcal{R}_{I_i}(\tau)\right)$$

$$\simeq (30)^2\frac{11}{12}\mathcal{R}_{I_i}(\tau)$$

$$\Rightarrow$$

$$\mathcal{S}_{D_i}(\omega) \simeq (30)^2\frac{11}{12}\mathcal{S}_{I_i}(\omega)$$

$$(9)$$

Pulling everything together, after reconstructing the detector signals ($600\ I_i = D_{d,i} + 10\ S_d$), we have

$$(600)^2\ \sigma^2(V) = \frac{2}{T}\int_0^T \left(1 - \frac{\tau}{T}\right)\left(\mathcal{R}_{D_{d,i}}(\tau) + (10)^2\ \mathcal{R}_{S_d}(\tau)\right)\ d\tau$$

$$= (600)^2\frac{2}{T}\int_0^T \left(1 - \frac{\tau}{T}\right)\left(\frac{11}{12}\mathcal{R}_{I_i}(\tau) + \frac{1}{12}\mathcal{R}_{I_i}(\tau)\right)\ d\tau$$

$$= (600)^2\frac{2}{T}\int_0^T \left(1 - \frac{\tau}{T}\right)\mathcal{R}_{I_i}(\tau)\ d\tau$$

Under the assumptions made, regarding the equality of the noise levels in each detector, the sum and difference amplifiers have no effect on the noise as seen in the data stream. Even though, the noise in the sum and difference channels is lower than the levels seen in the respective detector signals. Theoretically, this is simply a result of better statistics when combining several detectors into the noise calculation.

So from this, using equation 6, the *rms* width we expect to see in the data is

$$
\begin{aligned}
\sigma(V) &= \sqrt{\frac{4k_B T_k R}{\pi \ RCT}} \sqrt{\int_0^T d\tau \left(1 - \frac{\tau}{T}\right) \int_{-\pi/2}^{\pi/2} d\theta \frac{\cos\left(\frac{\tau}{RC}\tan\theta\right)}{(1+\tan^2\theta)^5}} \\
&= \sqrt{4k_B T_k R}\sqrt{B}\sqrt{\Phi}
\end{aligned}
$$

(10)

Here B is the bandwidth which must be used in the determination of the expected noise. It is always the inverse of the chosen sampling interval T. The integral

$$
\Phi = \frac{1}{\pi \ RC} \int_0^T d\tau \left(1 - \frac{\tau}{T}\right) \int_{-\pi/2}^{\pi/2} d\theta \frac{\cos\left(\frac{\tau}{RC}\tan\theta\right)}{(1+\tan^2\theta)^5}
$$

can be calculated numerically. In the case where the time bin is taken to be the sampling interval ($T = 0.4 \ ms$) it evaluates to $0.77019 \pm 8.6 \times 10^{-5}$.

The resistance values used in equation 10 are different for each detector (See section 3.4). The results for the noise seen in the detectors are shown in figure 21 (blue). The noise calculated from equation 10 is shown in red. The fact that some of the detectors show slightly
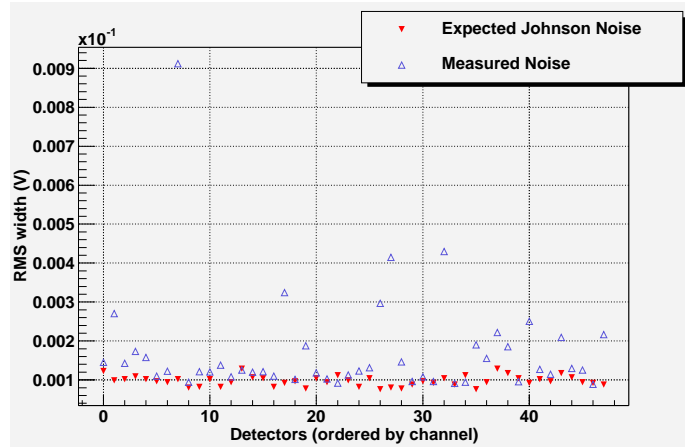

Figure 21: Noise levels for each detector.

lower than expected noise levels is likely due to the approximations made in the derivation of the expected noise above. Noise significantly above the expected levels probably originates from capacitive coupling on the detector preamplifier boards, due to dirt or cold solder joints.

4.1.2 False Asymmetry

There are three important test that will establish whether or not there are any large systematic errors regarding the detector electronics and the spin flipper. The first serves to establish the time required to measure the asymmetry due to electronic noise down to the

desired accuracy without the spin flipper running. The second measures the same thing with the spin flipper running to see if there are any effects. This test will look for an additive effect, that is, for and addition to the signal due to spin flipper correlated electronic pickup. The third test will look for a multiplicative effect the spin flipper magnetic field will have on the VPD gain. That is, for spin flipper correlated gain change. This can only be seen by having a signal (light) going into the VPD. This is accomplished by turning on the LEDs in each detector so that their light output is approximately equal to the scintillation light seen during beam on measurements and then performing the same asymmetry measurement as before, again with the spin flipper running.

In the analysis, one asymmetry per time bin is calculated. Let (U,D) be one detector pair 180 degrees apart. Here, $U(U)$ refers to the upper (lower) detector, with respect to its position in the array. Let $(U_\uparrow, U_\downarrow)$ denote the sum of all four signals, in a given spin sequence, in which the neutron was in the spin up state and the spin down state respectively. Then the asymmetry for a given time bin is calculated from

$$A_\gamma = \frac{1}{d}(U_\uparrow - D_\uparrow - U_\downarrow + D_\downarrow).$$

Here, the denominator depends on several factors. First, the overall gain in the sum and difference amplifiers and the summing scheme in the DAQ system, which was discussed above, enters with a factor of 600. Next, there are 8 individual measurements from 2 detectors each included in the calculation, producing a factor of 16. The last component is the expected average ADC count seen for a detector during beam on measurements. This number can be estimated from flight path beam brightness measurements and Monte Carlo predictions (See section 1) [1]. The predicted rate of γ-rays into the entire array is $\simeq 50MHz$. From this, the detector efficiency (See section 3.1) and from our knowledge of the gain factors in the preamplifiers, the expected ADC count in a single detector is $\simeq 5 \times 10^3$. So the denominator value used in the asymmetry calculation is $d = 4.8 \times 10^7$. Several data runs contribute to the asymmetry measurements and for each detector pair in the array a combined mean and standard deviation is calculated from all runs. An error wighted average asymmetry is then calculated for all detector pairs.

Both for the spin flipper on and off (no LED) measurements, the time required to measure the asymmetry to a certain accuracy is governed by the rms with in the signal due to Johnson noise (eqn. 10) and additional noise from the detector preamplifier (See [7]). The spice model predicted noise levels for beam-off and LED off measurements is $\simeq 21\ \mathrm{fA}/\sqrt{\mathrm{Hz}}$ and the analysis in section 4.1.1, regarding the noise as seen from the data stream then predicts an expected average RMS width of $\simeq 0.1$ mV.

In this mode, the asymmetry can be measured down to 5×10^{-9} level in about 3 hours of run time. The individual detector pair asymmetries from the spin flipper runs are shown in figure 22. In about 5 hours of run time, the asymmetry with the spin flipper was measured to

$$A_\gamma = (-1 \pm 3) \times 10^{-09}.$$

The noise in the detectors, seen with the spin flipper running, did not significantly change from those shown in figure 21.
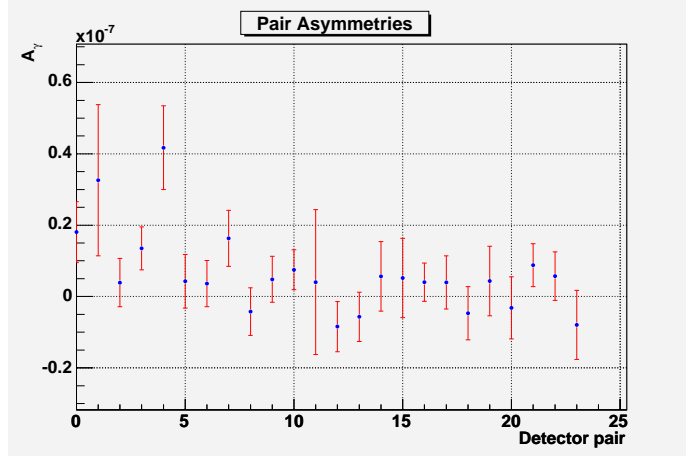
Figure 22: Asymmetry results (spin flipper on, LEDs off)

When the LEDs are turned on, the rms width of the detectors signals is dominated by shot noise at the photo-cathode. If the shot noise is characterized by a single electron as the fundamental quantum of charge, then the expected average noise is $\simeq$ 95 fA/$\sqrt{\text{Hz}}$ at an average current of 28 nA out off the VPDs. The asymmetry for the 24 detector pairs with LED signal is shown in figure 23.
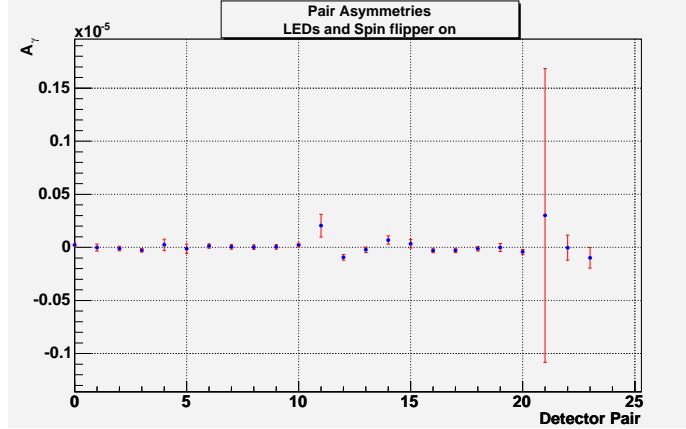

Figure 23: Asymmetry results (spin flipper on, LEDs on)

In about 11 hours of run time, the asymmetry with the LED signal was measured to

$$A_\gamma = (-8 \pm 5) \times 10^{-09}.$$

The noise in the detectors, seen with the LEDs turned on is shown in figure 24.

5   Conclusion

From the theoretically expected noise in the detector preamplifier, the runtime necessary to measure the beam-off, LED-off asymmetry to 5×10^{-9} is predicted to be $\simeq$ 1 hour. From the theoretical estimate of the shot noise for LED-on measurements, the runtime should be $\simeq$ 5 hours for the 28 nA average photo-current selected. The tests performed show that the run-times necessary are actually 2 to 3 times higher than the predictions. However,
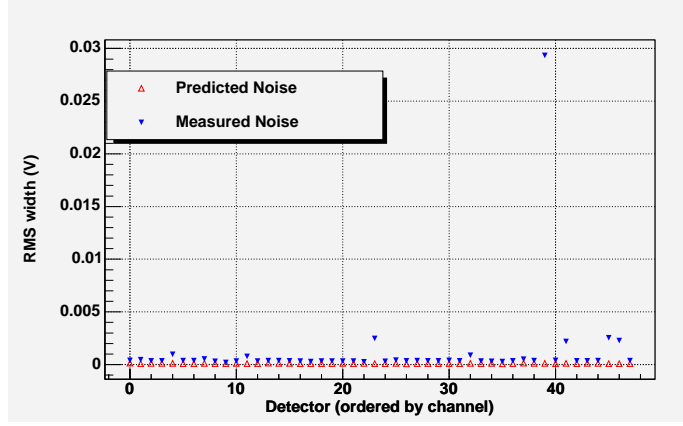
Figure 24: Noise levels for each detector with LEDs turned on

the average beam-off noise in the preamplifier as seen in figure 21 is $\simeq 37\mathrm{fA}/\sqrt{\mathrm{Hz}}$, about 85% higher than expected and the runtime required with this noise level corresponds to $\simeq 3$ hours. The same is seen to be true for the LED-on (Beam-on) measurement.

These results show that the detector array is operating as designed and fulfills all criteria needed to perform a successful measurement of the γ asymmetry. Specifically, the beam-off LED-off additive asymmetry due to spin flipper correlated electronic pickup as well as the LED-on multiplicative asymmetry due to spin flipper correlated gain changes in the VPD were measured to the desired level of accuracy within a reasonably short time and were consistent with 0.

6   Dynode Corrections

7   Tables and Miscillaneous Information

7.1   Tables

Table 1: Cesium Iodide
Properties for common dopant

	CsI(Tl)	CsI(Na)	CsI(undoped)
Density $[g/cm^3]$	4.51	4.51	4.51
Melting Point $[K]$	894	894	894
Thermal expansion coefficient $[K^{-1}]$	$54e^{-6}$	$49e^{-6}$	$49e^{-6}$
Cleavage plane	none	none	none
Hardness (Mho)	2	2	2
Hygroscopic	slightly	yes	slightly
Wavelength of emission maximum $[nm]$	550	420	315
Lower wavelength cutoff $[nm]$	320	300	260
Refractive index at emission maximum	1.79	1.84	1.95
Primary decay time $[\mu s]$	1	0.63	0.016
Afterglow (after 6 ms) $[\%]$	0.5-5.0	0.5-5.0	—
Light yield $[photons/MeV\,\gamma]$	$52-56e^3$	$38-44e^3$	$2e^3$
Photo-electron yield $[\%\,of\,NaI(Tl)]$ (γ rays)	45	85	4-6
Absolute Scintillation Efficiency for Fast Electrons	11.9%	11.4%	—

References

[1] P.N. Seo et al. A measurement of the flight path 12 moderator brightness at lansce. *Nucl. Instr. and Meth. A (accepted)*, 0:0, 2003.

[2] T. B. Smith et al. A radio frequency spin flipper for polarized neutrons from a spallation source. *NPDGamma Internal Note*, 0, 2001.

[3] Glenn F. Knoll. *Radiation Detection and Measurement.* John Wiley & Sons, New York, 1989.

[4] Davenport W. B. Root W. L. *An Introduction to the Theory of Random Signals and Noise.* Wiley Interscience and IEEE, New York, 1987.

[5] W. R. Leo. *Techniques for Nuclear and Particle Physics Experiments.* Springer-Verlag, New York, 1987.

[6] Horowitz P. Hill W. *The Art Of Electronics.* Cambridge University Press, New York, 1982.

[7] W. S. Willburn. The npdgamma low-noise preamplifier. *NPDGamma Internal Note*, 0, 2002.

[8] Ino Takashi Muto Suguru Masuda Yasuhiro. Note on vacuum photodiode calibration at kek. *NPDGamma Internal Note*, 0, 2002.